Prediction of Solvent Effects on Vibrational Absorption Intensities and Raman Activities in Solution within the Polarizable Continuum Model: A Study on Push−Pull Molecules

Stefano Corni,[†] Chiara Cappelli,*[,‡] Mirella Del Zoppo,[§] and Jacopo Tomasi[‡]

INFM Center for nanoStructure and bioSystems at Surfaces (S[3]), Dipartimento di Fisica, Università di Modena e Reggio Emilia, via Campi 213/A, I-41100 Modena, Italy, Dipartimento di Chimica e Chimica Industriale, Università di Pisa, via Risorgimento 35, I-56126 Pisa, Italy, and Dipartimento di Chimica Materiali e Ingegneria Chimica, Politecnico di Milano, Piazza Leonardo Da Vinci 32, I-20133 Milano, Italy

Received: April 10, 2003; In Final Form: September 15, 2003

We present a comparison between experimental and calculated vibrational infrared and Raman spectra (harmonic frequencies, absorption intensities, and scattering activities) for two push−pull molecules, [(2*E*,4*E*)-5-(dimethylamino)penta-2,4-dienylidene]malononitrile and 5-[(2*E*,4*E*)-5-(diethylamino)penta-2,4-dienylidene]-1,3-diethylpyrimidine-2,4,6(1*H*,3*H*,5*H*)-trione, widely studied for their nonlinear optical properties, in several solvents. The polarizable continuum model (PCM) has been used to describe the solvents, and the molecules have been treated at the density functional theory (DFT) level. Local field effects on IR intensities and Raman activities are included in the calculations. Solvent effects on absorption and scattering intensities are predicted fairly well. A number of reasons for discrepancies between calculated and experimental results are discussed. The variation of the bond length alternation (BLA) of the studied molecules as a function of the solvent is also discussed.

1. Introduction

Push−pull molecules are characterized by the presence of three main elements: an electron-donor group (push), an electron-acceptor group (pull), and a polarizable π electron group which connects the push and the pull parts of the molecule. Such molecules have been widely studied for their possible applications in the field of nonlinear optics and electro-optics.[1,2] In fact, by varying the electron-donor or -acceptor capability of the push and pull groups, sizable variations in the hyperpolarizability of the molecule (and, consequently, in the nonlinear susceptibility) are expected and indeed observed.

For the fine-tuning and optimization of nonlinear optical properties, the strategy of modifying the chemical nature of the push−pull groups is not convenient, because "quantized" variations in the properties are obtained. Because of their polar nature, push−pull molecules are extremely sensitive to the environment. This sensitivity can be exploited for the tuning of their nonlinear optical properties simply by varying the solvent in which they are immersed.

Due to the technological interest in push−pull molecules, several experimental and theoretical studies have been performed on them. In particular, in this paper we will focus on the study of vibrational infrared (IR) and Raman spectra of a couple of representative cases. As we have previously remarked, optical properties of push−pull molecules are strongly sensitive to the environment: thus, a large solvent dependency of vibrational spectroscopic properties is expected, which, indeed, has been pointed out by experimental evidences collected in refs 3.

Some of the authors of the present article have recently proposed methodologies for the theoretical treatment of solvent effects on infrared absorption intensities[4,5] and Raman scattering activities[6−8] within the framework of the polarizable continuum model (PCM).[9,10] In this model the solute molecule is treated quantum-mechanically (for example at the Hartree−Fock, HF, or at the density functional theory, DFT, level) and the solvent is modeled as a homogeneous and infinite continuum dielectric hosting a cavity where the solute is embedded.

The interest in studying push−pull molecules with such methodologies and to compare the results with experimental findings is at least twofold: on one hand, the comparison in the case of quite complex molecules can help in validating the theoretical model, pointing out its qualities but also its limits; on the other hand, a theoretical study can deliver information which cannot be obtained from the experiment. For example, it is possible to analyze in more detail changes in solute properties induced by the solvent, elucidating which, among the various solvent effects (such as induced changes in the solute equilibrium geometry, in the polarity of the solute, or in the local field acting on it), determines the variations in the properties.

Among the large variety of molecules studied in ref 3, we have chosen to work with the two depicted in Figure 1, [(2*E*,4*E*)-5-(dimethylamino)penta-2,4-dienylidene]malononitrile and 5-[(2*E*,4*E*)-5-(diethylamino)penta-2,4-dienylidene]-1,3-diethylpyrimidine-2,4,6(1*H*,3*H*,5*H*)-trione, from now on called M1 and M2. The choice has been made by tuning the size of the molecules and the possibility of performing computations at a reasonable level of accuracy. In addition, M1 and M2 show a particularly strong dependency of vibrational absorption and Raman scattering activity on the nature of the solvent. Such a strong dependency makes these two molecules good candidates to test the quality of the theory presented in refs 4−6.

The article is organized as follows: in the next section

* Corresponding author. E-mail: chiara@dcci.unipi.it. Current affiliation: INFM, Unità di Ricerca di Pisa, c/o Dipartimento di Chimica e Chimica Industriale, Università di Pisa, via Risorgimento 35, I-56126 Pisa, Italy.

[†] INFM-S[3].

[‡] Università di Pisa.

[§] Politecnico di Milano.

10.1021/jp034960u CCC: $25.00
Published on Web 11/07/2003

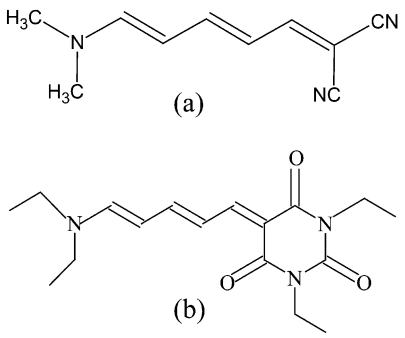

Figure 1. Chemical structures of the two molecules considered in the present work: (a) M1; (b) M2.

(Theory) we shall give a brief summary of the methodologies discussed in refs 4−6. Then, in the Experimental Section a description of the techniques used to collect the experimental data will be given. Finally, in the Results and Discussion section, we shall compare experimental and calculated IR absorption intensities and Raman activities for the two molecules. In that section we shall also discuss, in the light of the calculated results, the solvent induced effects on these molecules.

2. Theory

Expressions for both vibrational absorption intensities and vibrational Raman scattering activities can be derived in the framework of the semiclassical theory of light/matter interaction by resorting to time dependent perturbation theory.[11] The most important term in the perturbation expressing the interaction between the molecule and the radiation is the dipolar one. For molecules in the gas phase, such a term is simply $-\vec{\mu}\cdot\vec{E}$, where $\vec{\mu}$ is the molecular dipole moment and $\vec{E}$ is the electric field associated with the radiation, measured at the position of the molecule.

In the case of a molecule in solution and assuming that the solvent is described as a continuum dielectric, the leading term in the interaction among the molecule and the electromagnetic field is to be expressed as $-(\vec{\mu}+\tilde{\vec{\mu}})\cdot\vec{E}^{\mathrm{M}}$,[4] where $\vec{\mu}+\tilde{\vec{\mu}}$ is the so-called *external dipole moment* introduced by Onsager[12] and $\vec{E}^{\mathrm{M}}$ is the macroscopic electric field associated with the radiation in the solvent medium. The external dipole moment is the sum of the dipole moment of the molecule ($\vec{\mu}$) and the dipole moment induced by the molecule in the solvent ($\tilde{\vec{\mu}}$).

In the framework of PCM, $\tilde{\vec{\mu}}$ (or, better, its matrix elements) can be calculated by solving an integral equation defined on the boundary of the cavity hosting the solute.[4] Such an integral equation becomes a matrix equation once the cavity boundary is discretized and then the matrix equation is solved with standard techniques.

The application of perturbation theory to molecules in solution yields expressions for vibrational absorption intensities and Raman scattering activities very similar to those for isolated molecules, but involving $\tilde{\vec{\mu}}$. In the double (electric and mechanical) harmonic approximation, the integrated absorption coefficient A^{sol} for the i-th vibrational mode reads[4]

$$A^{\mathrm{sol}} = \frac{\pi N_{\mathrm{A}}}{3 n_{\mathrm{sol}} c^2} \left|\frac{\partial(\vec{\mu}+\tilde{\vec{\mu}})}{\partial Q_i}\right|^2 \tag{1}$$

where N_{A} is Avogadro's number, n_{sol} is the refractive index of the pure solvent at the frequency of the vibrational transition, and c is the light velocity. Q_i is the (mass-weighted) normal coordinate associated with the i-th vibrational mode.

The exact expression for the Raman scattering intensity depends on the directions of the incident light beam and of the light scattering collection. By assuming that (1) the incident light is polarized perpendicularly to the scattering plane, (2) the scattered light is collected perpendicularly to the direction of incidence, and (3) only the component of the scattered light that is polarized as the incident field is measured, the radiant intensity of the i-th Stokes band for a molecule in solution, $I_{\mathrm{R}}^{\mathrm{sol}}$, is

$$I_{\mathrm{R}}^{\mathrm{sol}} = \frac{\hbar k^4}{2\omega_i} I_0 \frac{45\alpha'^2 + 4\gamma'^2}{45} \tag{2}$$

where

$$\alpha'^2 = \frac{1}{9}\left(\sum_r \frac{\partial \alpha_{\mathrm{rr}}^*}{\partial Q_i}\right)^2 \tag{3}$$

$$\gamma'^2 = \frac{1}{2}\left[3\sum_{rs}\left(\frac{\partial \alpha_{\mathrm{sr}}^*}{\partial Q_i}\right)^2 - 9\alpha'^2\right] \tag{4}$$

The double harmonic and the Placzek approximations have been assumed.[13,14] In eq 2, ω_i is the angular frequency of the vibrational mode under study and Q_i is the corresponding normal coordinate. The quantities α'^2 and γ'^2 are invariants of the derived-polarizability tensor $\partial\bar{\alpha}^*/\partial Q_i$. The elements of $\bar{\alpha}^*$, the effective polarizability for the molecule is solution, can be written as[6]

$$\bar{\alpha}_{\mathrm{rs}}^*(-\omega',\omega') = -\sum_{R\neq 0} \frac{\langle 0|\mu_{\mathrm{r}} + \tilde{\mu}_{\mathrm{r}}|R\rangle\langle R|\mu_{\mathrm{s}} + \tilde{\mu}_{\mathrm{s}}|0\rangle}{\hbar(\omega_{\mathrm{R0}} - \omega')} + \frac{\langle 0|\mu_{\mathrm{s}} + \tilde{\mu}_{\mathrm{s}}|R\rangle\langle R|\mu_{\mathrm{r}} + \tilde{\mu}_{\mathrm{r}}|0\rangle}{\hbar(\omega_{\mathrm{R0}} + \omega')} \tag{5}$$

where the R index runs over the electronic excited states of the molecule in solution, ω_{R0} are the electronic excitation energies, and ω' is the frequency of the incident radiation.

In the present article, we shall calculate $\bar{\alpha}^*$ by using the time dependent density functional theory (TDDFT) and we shall obtain the derivatives $\partial\bar{\alpha}^*/\partial Q_i$ by numerically differentiating $\bar{\alpha}^*(-\omega',\omega')$ with respect to a displacement along the normal coordinate Q_i. Note that recently an analytical method for the evaluation of these derivatives at the time dependent Hartree−Fock level has been proposed.[15]

A quantity which is used to estimate the intrinsic capability of a molecule to scatter light, besides the trivial k^4 factor, is $|R|$, defined for the i-th band as[16]

$$|R_i|^2 = \frac{I_{\mathrm{R}}^{\mathrm{sol}}}{I_0}\frac{2\omega_i}{\hbar k^4} = \frac{45\alpha'^2 + 4\gamma'^2}{45} \tag{6}$$

This is the quantity which will be calculated for the two molecules under study and which will be compared with experimental measures.

The first equality in eq 6 could be directly exploited to obtain the experimental value of $|R_i|$ because all the quantities in the right-hand term can be measured. However, the absolute measurement of radiation intensities is a quite delicate task, and it would be extremely ineffective to perform such a difficult measure for several solutes in several solvents. The estimation of intensity ratios between bands belonging to the same spectrum

TABLE 1: Radii of the Spheres Used to Build the Molecular Cavity for PCM Calculations

atom	radius (Å)
CH_3	2.40
CH	2.28
O	1.86
N	2.04

is much easier. Thus, if a band of the solvent is chosen as reference and its absolute intensity is evaluated once, then solute absolute intensities can easily be extracted from relative intensities with respect to that band. Basically, this is the procedure used to obtain experimental data discussed later in this paper (see ref 16 for details). We remark, however, that our calculated $|R|$ values (obtained through the second equality of eq 6) already take into account solvent effects, and thus, $|R|$ in the present paper is equal to that defined in ref 16 times the semiclassical local field correction L^s defined there.

For both Raman scattering and infrared absorption calculations, we shall assume a nonequilibrium model for the dielectric response of the solvent. Such a model, which is presented in ref 5 for infrared absorption and in ref 7 for Raman scattering, is based on the idea that the solvent cannot instantaneously readjust to the oscillations in time of the solute charge density. These oscillations can be due either to solvent vibrations (mattering for both infrared and Raman) or to the polarization induced in the solute by the incident electromagnetic field (mattering only for Raman). In the present study we shall use the models presented in refs 5 and 7 to take into account such a nonequilibrium response.

2.1. Computational Details. All the calculations have been done with the density functional theory by using the hybrid functional B3LYP as implemented in Gaussian[17] and the 6-31+G* basis set, with the exception of frequencies and normal modes for M2, that were calculated with the 6-31G* basis set. These basis sets guarantee a reasonable compromise between accuracy and computational costs.[18,19]

For calculations in solution, we have treated the solvent with the PCM, in the integral equation formalism (IEF) formulation,[20] which is able to model solvent effects on various molecular properties.[21] The molecular shaped cavity in which the molecule is hosted is built in terms of interlocking spheres centered on each atom except hydrogens. The radii of the spheres are reported in Table 1.

The geometry of the molecules has been optimized in each medium by exploiting the analytical calculation of first-order energy derivatives (see ref 22). The methodology described in refs 5 and 23 has been used to calculate harmonic vibrational frequencies in solution. No scaling factors have been applied to calculated harmonic frequencies; that is, they are reported as obtained from the Gaussian output.

The solvents considered for M1 are benzene, chloroform, dichloromethane, acetonitrile, and methanol; those considered for M2 are tetrachloromethane, chloroform, dichloromethane, acetonitrile, and nitromethane.

For the calculations of Raman activities, we have considered only the bands for which the experimental $|R|$ was measured. We have thus developed a procedure to compute the Raman intensity from the effective Raman electronic polarizability ($\bar{\alpha}^*$) which works band by band. This permits a remarkable saving of computational time when only a small portion of the spectrum or some selected bands are of interest. In addition, for M2 we could calculate normal modes with the 6-31G* basis set and Raman intensities with the 6-31+G* one. The possibility of using two different basis sets for frequencies and Raman intensities is a quite useful feature of our implementation, which permits us to improve the overall cost/accuracy ratio by choosing separately the basis set proper for the two quantities.

As the large size of the molecule M2 implies very large computational costs, in the case of Raman calculations we have simplified it by replacing all the ethyl groups (two on the terminal amino group and two on the ring nitrogen atoms) by methyl groups. We remark that for IR calculations the actual M2 molecule has been considered. All the Raman activity calculations have been done by assuming an incident light wavelength of 1064 nm (the same as in the experiment).

3. Experimental Section

The infrared and Raman absolute intensities of the molecules considered in this work (M1 and M2), dissolved in all the solvents for which calculations have been carried out, have been experimentally measured.

Infrared measurements were made with a FT-IR interferometer Nicolet 7000 equipped with a MCT detector in the spectral range 4000−400 cm^{-1}. Raman measurements were made with a FT-Raman interferometer Nicolet 910 with an Nd:YAG laser ($\lambda_{exc} = 1064$ nm) and a near-IR germanium detector. All spectra were corrected for the wavelength dependence of the detection efficiency using a standard lamp.

The determination of the absolute infrared intensity of the *i*-th band of a sample in solution is simply obtained from the integrated absorbance according to the following equation:

$$A_i = \frac{1}{cl}\int_{i\text{-th band}} \mathrm{d}\nu \ln\left(\frac{I_0}{I}\right) \tag{7}$$

where I_0 and I are the incident and the transmitted light intensities, respectively. Solution concentrations c of the order of a few milligrams per milliliter or less and cell thicknesses l of the order of 0.1 mm were used.

The measure of the absolute Raman cross sections is more problematic. It can be strongly affected by various experimental conditions: most of the problems can be overcome with the use of an internal intensity standard whose absolute cross section is accurately known. Kato et al.[24] have measured the absolute Raman intensities of several organic solvents by direct comparison with the blackbody emission at known temperature.

To obtain experimental absolute Raman intensities, we must measure the term $|R_i|^2$ appearing in eq 6, which is given by a proper combination of the invariants of the Raman tensor relative to the *i*-th Raman transition. The expression in eq 6 refers to Raman experiments carried out with incident and scattered light with mutually parallel electric vectors.

Let a_i^s be the experimental area of the *i*-th Raman band of the molecule under study at frequency ω_i^s and a_i^r be that of the "reference" band of the solvent at ω^r. We can define the ratio x_i

$$x_i = I_i^s/I^r = \frac{a_i^s}{c^s}/\frac{a^r}{c^r} \tag{8}$$

where c^r/c^s is the molar ratio between the reference molecule (solvent) and the sample. Comparing the above expression and eq 6, it is apparent that $|R_i|^2$ of the molecule can be determined from the knowledge of x_i, $|R|^2$ of the reference band of the solvent, the vibrational frequencies of the *i*-th band of the sample and of the reference band, and the ratio of the k factors of eq 6. In our measurements we generally used sample concentrations $\approx 10^{-5}$ mol cm^{-3}.

The choice of using an exciting line in the IR has been made in order to avoid resonance or preresonance effects. This means that since the reference values $|R|^2$ were obtained with laser excitation in the visible range, values relative to $\lambda_{exc} = 1064$ nm have been extrapolated. This has been done using the relationship proposed by Kato, assuming that only one excited electronic state is relevant in the Raman process.

In our experiments, in order to have intensity data for the largest choice of common organic solvents, we had to also use solvents for which absolute cross sections were not available. In these cases reference values of $|R_i|^2$ of other solvents have been obtained by making a binary solution of CCl_4 and the unknown solvent, which in this case plays the role of the sample molecule. The reliability of this technique was tested on a mixture of CCl_4 and benzene. The values thus obtained for benzene are very close to those reported in ref 24.

4. Results and Discussion

In this section we will show a comparison of calculated and experimental IR absorption intensities and Raman scattering coefficients for M1 and M2 in various solvents. We will consider IR intensities and Raman activities separately for each molecule. Both a qualitative (spectrum appearance) and a quantitative (absolute intensities) comparison between calculated and experimental results will be performed. The frequency values reported in the text refer to experiments, unless differently stated.

4.1. Vibrational Infrared Absorption. *4.1.1. M1.* In Figure 2a and b we report a picture of calculated infrared spectra of M1 in benzene and acetonitrile obtained by considering Lorentzian band shapes and a bandwidth parameter of 10 cm^{-1} common to all bands. In Figure 2c and d, the corresponding experimental spectra are reported. The qualitative agreement in benzene is good, both in terms of frequencies (which, as usual, are overestimated by harmonic DFT calculations)[25] and in terms of relative intensities. The presence of two bands [labeled (1)] in the CN stretching region ($\approx$2200 cm^{-1}) for the calculated spectrum depends on a slight overestimation of the splitting between the symmetric and the antisymmetric stretches of the two nitriles. The shape of the experimental band suggests the presence of two almost coincident peaks as well. We also remark on the good agreement between calculated and experimental spectra in the regions from 1500 to 1700 cm^{-1}, where the most intense peaks are present [(2) and (3)], and from 1150 to 1500 cm^{-1} (compare Figure 2a and c). The shape of the experimental pattern of the latter is well reproduced by the calculation [peak (4) is hidden by peak (5)]. The intensities of peaks around 800 cm^{-1} are strongly underestimated by the calculations: anharmonicity is probably relevant in this region.

Moving to the spectrum in acetonitrile (Figure 2b and d), the most evident change in the experimental spectrum (Figure 2d) is the decrease in the relative intensity of band (2), which is not predicted by the calculation. In addition, peaks (5) and (6) increase their overlap. Such a trend is overestimated by the calculated spectrum (Figure 2b), where the two peaks overlap almost completely. This overlapping is the origin of the strong band at 1230 cm^{-1} present in the calculated spectrum, given by (4) + (5) + (6); this is the main difference with the experimental spectrum.

From the experimental spectra of M1 in the various solvents, several vibrational frequencies and infrared absorption coefficients were extracted. This allows an extensive comparison of experimental and calculated data. The frequency values of the bands which will be considered to perform such a comparison are grouped in Table 2. Notice that such frequencies refer to spectra recorded in benzene and acetonitrile, which are representative of nonpolar and polar solvation environments, respectively.

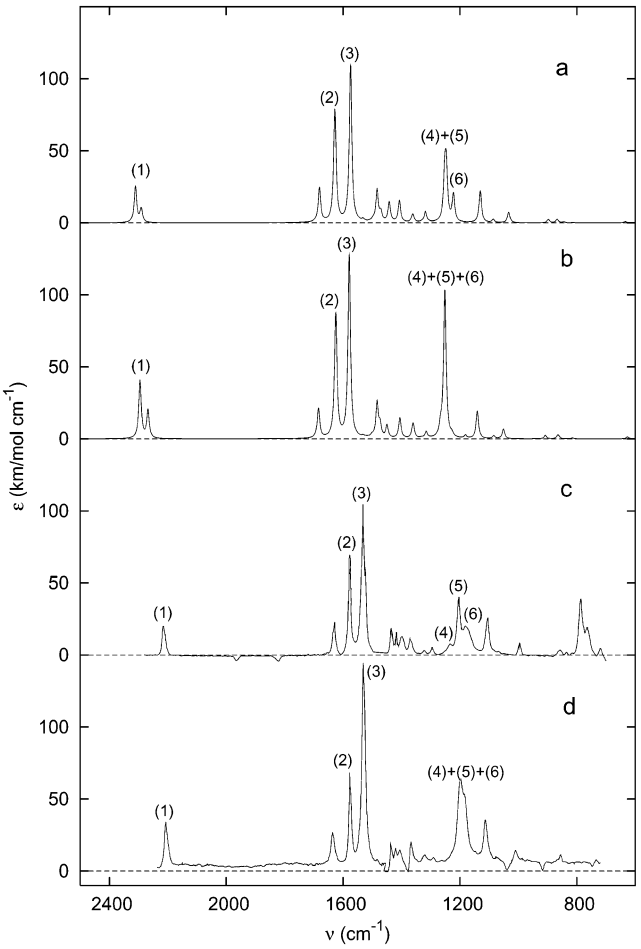

Figure 2. Calculated and experimental IR spectra of M1 in benzene (a, c) and acetonitrile (b, d). All the calculated spectra are obtained by considering Lorentzian-shaped bands with a bandwidth of 10 cm^{-1}.

TABLE 2: IR Vibrational Frequencies Measured for Selected Bands of M1 in Benzene and in Acetonitrile[a]

benzene	acetonitrile	exp shift	calc shift
2215	2207	−8	−18
1630	1635	5	3
1577	1574	−3	−3
1530	1529	−1	5
1433	1434	1	0
1367	1367	0	−1
1294	1290	−4	−2
1203	1198	−5	11
1181	1184	3	5
1105	1113	8	9

[a] "Shift" is the difference between values in acetonitrile and in benzene, experimental (exp) or calculated (calc). Values are given in cm^{-1}.

As can be seen, frequency shifts moving from one solvent to another are quite small (maximum shift: 8 cm^{-1}). Such differences are comparable to errors ascribed to the computational level we are using, and thus, a comparison of calculated and experimental solvent effects for vibrational frequencies is not completely meaningful. Anyway, we have reported in Table 2 the computed frequency shifts passing from benzene to acetonitrile. We just note that the sign and the relative magnitude of the shift are usually well reproduced, with the exception of the band at 1203 cm^{-1}.

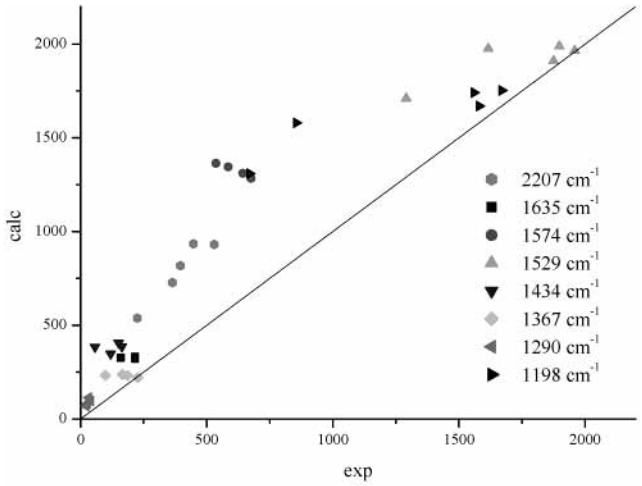

Figure 3. Comparison between calculated (calc) and experimental (exp) IR absorption intensities for different bands of M1 in different solvents. Values are in km mol^{-1}.

TABLE 3: Integration Range for IR Intensities of the Various Bands of M1[a]

band (cm^{-1})	range (cm^{-1})	band (cm^{-1})	range (cm^{-1})
2207	2226−2183	1434	1439−1426
1635	1650−1619	1367[b]	1384−1346[b]
1574	1590−1558	1290	1299−1280
1529	1554−1505	1198	1234−1151

[a] The values refer to the infrared spectrum in acetonitrile. [b] Values for methanol.

Moving to vibrational absorption coefficients, we note that they are by far more sensitive to the solvent than vibrational frequencies (variations of a factor of 2 are measured for both M1 and M2). These variations are larger than the experimental error, that we estimate is around ±5−10%. Thus, in this case the comparison between theory and experiments should be meaningful and adequate to evaluate the capability of the methodologies developed in refs 4 and 5 of reproducing experimental solvent effects. We remark that in some cases it was not possible to integrate separately overlapping peaks and that, although we shall refer to a *band* and to the corresponding frequency, we may actually mean a group of overlapping bands.

In Table 3 we report the integration range for each band, labeled by the frequency of the most prominent peak in the spectrum in acetonitrile. For other solvents the range changes a little, but the vibrational modes included in a given range are the same.

To make the comparison between experiments and calculations meaningful, we will report calculated data as the sum of the coefficients of all the vibrational modes included in the integration range. Due to the strong resemblance between experimental and calculated spectra, the choice of such modes has been done unambiguously.

We have experimentally examined eight bands for each of the five solvents, for a total of 40 absorption coefficients. Actually, the number of experimental absorption coefficients is somewhat smaller, 35, due to the fact that it was not possible to accurately measure the coefficients of some bands in some solvents. A synthetic way of expressing data and performing the experiment−computation comparison is to group them in a single correlation graph, using the same symbol for results connected to the same band. Such a graph is reported in Figure 3.

As can be seen, our calculations usually overestimate the experimental infrared intensity, in some cases even by 50−60%.

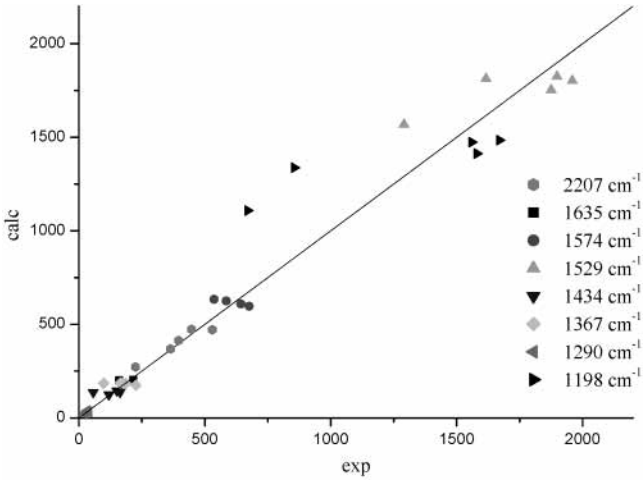

Figure 4. Comparison between calculated (calc) and experimental (exp) IR absorption intensities for different bands of M1 in different solvents. Calculated results are scaled as explained in the text. Values are in km mol^{-1}.

The differences between experiment and theory may depend, among the other causes, on both the solvation model and the intrinsic level of accuracy of a B3LYP/6-31+G* calculation within the double harmonic approximation. In this paper we are particularly interested in the effectiveness of the solvation model, and thus, we have tried to approximately decouple these two causes. To do that, we have assumed that for a given band the effect of the solvent is to multiply the infrared intensity of the molecule in the gas phase by a proper solvent dependent constant. In our opinion such an assumption is reasonable: in fact, theories for rationalizing solvent effects on infrared intensities, which have been developed within the Onsager theory,[26] model the solvent effect in terms of a factor dependent on the dielectric constant which multiplies the intensity of the isolated molecule.[27] By making such an assumption, the effect of the level of calculation is all charged on a hypothetical intensity in the gas phase from which intensities in solution are derived. If we further assume that such an intensity is α times the correct one, then all the intensities relative to a given band would be α times those reported in Figure 3.

One possibility to find α would be to choose a solvent as a reference and to obtain α for a given band as the ratio $A_{exp}^{ref}/A_{calc}^{ref}$ for that band. However, we have no reason to privilege one solvent over the others, and we prefer to fit the data, band by band, with a straight line crossing the origin (i.e., $A_{calc} = (1/\alpha)A_{exp}$) and to scale the calculated data with the α value obtained in such a way (note that each band has its specific value of α). Notice that other scaling procedures, for example, the use of "solvent specific" scale factors, could, in principle, be used (see ref 28 for an example in the case of vibrational frequencies). The result of the scaling procedure is depicted in Figure 4.

The correlation between experiment and theory is improved by the applied scaling. In particular, we would like to comment on the band at 2207 cm^{-1}, which can be easily assigned to the nitrile stretches. We remark that the calculated result is obtained by summing the intensities of the two peaks (1) present in the calculated spectra (see Figure 2). These bands (that in the experimental spectra appear as a single peak) are quite isolated from the others in the spectra, and thus, the sum of their intensities should be well reproduced by the calculation, because effects difficult to predict such as borrowing of intensity from other normal modes should not play an important role. In addition, the nitrile group is polar and conjugated with the rest

of the molecule, and thus, an appreciable sensitivity of its properties on the solvent is expected. Indeed, we found that experimental and computed results for such a band are in good agreement. The comparison is fairly good also for other bands with a large solvent dependency, such as the ones at 1198 and 1529 cm^{-1}.

The predicted solvent effect on the band at 1574 cm^{-1} is wrong, even qualitatively, showing a decrease in the intensity whereas an increase is experimentally observed. However, the intensity of this band is only moderately affected by the solvent, and for this reason, both errors on experimental values and limitations in the solvation model (such as the assumption of infinite dilution and the disregard of solute−solvent nonelectrostatic interactions) can play a decisive role. We also remark that in the case of the band at 1574 cm^{-1} the agreement between experiments and calculations is the worst in the series even before the scaling. One possible source of error in this case is the closeness of this band with the most intense one (1529 cm^{-1}): even a small error in the calculation of normal modes can transfer intensity from one band to the other. The less intense band is relatively more affected by this mixing. Finally, we note, as a general impression, a tendency of the calculation to overestimate the absolute value of infrared intensities and to underestimate solvent effects.

4.1.2. M2. The relative spatial arrangement of ethyl groups can originate different conformers of M2 having, possibly, similar energies. Thus, the overall spectrum may be thought of as the superposition of those of the various conformers, each weighted by the corresponding Boltzmann population. To check if this issue is relevant in the present case, energies and IR spectra of M2 in vacuo, in CCl_4, and in acetonitrile have been calculated by considering two conformations of the ethyl groups bonded to the ring nitrogen atoms and two conformations of the ethyl branches. We found that a variation in the conformation of ethyl groups bonded to the ring causes almost no variation in both energies and IR spectra. Different conformations of the ethyl groups of the amino group give different energies (approximately 2 kcal mol^{-1} in all the considered media) and somewhat different IR spectra. However, this energy gap ensures that, at room temperature, the experimental spectrum is almost exclusively due to the most stable conformer. Thus, we have performed the other calculations for the conformer having the lowest energy.

Among the solvents investigated herein, tetracholoromethane and acetonitrile are at opposite sides of the solvent polarity scale. Thus, we have chosen to perform the comparison of calculated (Figure 5a and b) and experimental (Figure 5c and d) spectra of M2 in these two solvents. The calculated spectrum in CCl_4 compares quite well with the experimental one. For peak (1) (at 1652 cm^{-1}), the experiment shows one peak and the calculation shows a double peak. However, the experimental peak is quite broad and can reasonably be composed of two overlapping peaks. Peak (3) appears to be the most intense one both in the calculated (Figure 5a) and in the experimental (Figure 5c) spectra. In the calculation, peak (4) is accompanied by a strong second peak, (5), which is much less intense in the experiment. As these two peaks are very close in frequency (19 cm^{-1} in the experiment and 12 cm^{-1} in the calculation), it is possible that a relatively small inaccuracy in the normal mode calculations has caused a redistribution of intensity between peak (4) and peak (5). This would also explain why peak (4) seems to have a smaller relative intensity in the calculation than in the experiment. The relatively small inaccuracy in frequency and normal mode calculations can also be responsible of the merging of peaks (6) and (7). By looking at calculated results in more detail, we actually found that the position of the two peaks is even inverted with respect to the experiment; that is, the peak with the largest intensity, (6), has the lowest frequency, not the highest. Their total height seems to be too large in comparison with the experiment. However, we note that in the experimental spectrum peak (6) is broader than other peaks, and thus, the comparison of heights does not actually correspond to a comparison of intensities (which are proportional to areas).

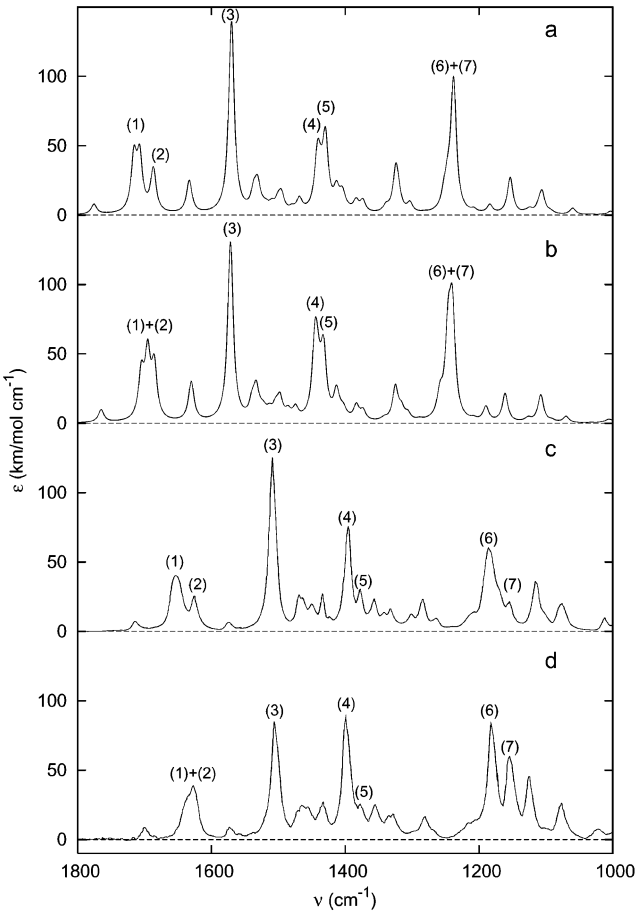

Figure 5. Calculated and experimental IR spectra of M2 in tetrachloromethane (a, c) and acetonitrile (b, d). All the calculated spectra are obtained by considering Lorentzian-shaped bands with a bandwidth of 10 cm^{-1}.

Moving from the experimental spectrum in CCl_4 (Figure 5c) to that in acetonitrile (Figure 5d), different changes in the overall appearance can be noted. In particular, we remark that (a) the relative intensity of peak (3) (1508 cm^{-1}) decreases with respect to the others [for example, the experimental intensity ratio (3)/(4) is 2.6 in CCl_4 and 0.99 in acetonitrile]; (b) bands (1) and (2) merge in a single peak; and (c) the relative intensity of the small peak at 1155 cm^{-1} [labeled (7)] increases. In the case of calculated spectra (Figure 5a and b), there is a decrease in the relative intensity of peak (3), but such a decrease is smaller than that in the experiment [e.g., the intensity ratio (3)/(4) is 3.9 in CCl_4 and 2.3 in acetonitrile]. Peaks (6) and (7) appear again as a single peak, as in CCl_4. However, their relative intensities change in changing the solvent: the calculated ratio between peak (6) and peak (7) intensities is 6.0 in CCl_4 and 1.3 in acetonitrile: this well reproduces the experimental trend. Also, the changes in peaks (1) and (2) are well reproduced by the calculation.

As for M1, the changes in experimental vibrational frequencies in passing from nonpolar to polar solvent are small and,

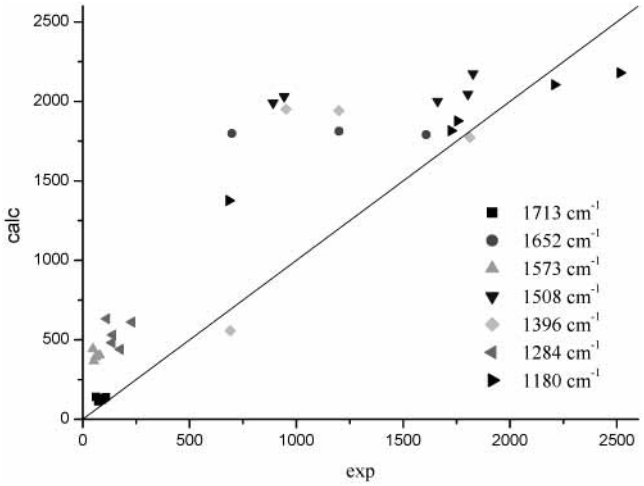

Figure 6. Comparison between calculated (calc) and experimental (exp) IR absorption intensities for different bands of M2 in different solvents. Values are in km mol^{-1}.

TABLE 4: IR Vibrational Frequencies Measured for Selected Bands of M2 in Tetrachloromethane and in Acetonitrile[a]

CCl_4	acetonitrile	exp shift	calc shift
1713	1700	−13	−11
1652	1627	−25	−18
1625	1627	2	−2
1573	1572	−1	−3
1508	1505	−3	2
1396	1399	3	2
1284	1282	−2	2
1186	1181	−5	1
1155	1155	0	−2

[a] "Shift" is the difference between values in acetonitrile and in tetrachloromethane, experimental (exp) or calculated (calc). Values are given in cm^{-1}.

TABLE 5: Integration Range for IR Intensities of the Various Bands of M2[a]

band (cm^{-1})	range (cm^{-1})	band (cm^{-1})	range (cm^{-1})
1713	1727−1702	1396	1413−1391
1652	1659−1615[b]	1284	1314−1271
1573	1595−1564	1186	1231−1135
1508	1547−1486	1077	1093−1063

[a] The values refer to the infrared spectrum in tetrachloromethane. [b] Values for dichloromethane.

again, a comparison between experimental and calculated frequency shifts is not completely meaningful. However, for the sake of completeness, we report in Table 4 experimental frequencies of M2 in tetrachloromethane and acetonitrile, together with calculated shifts. For the bands more sensitive to the solvent, calculated shifts are in good agreement with experiments. Some tests performed with a larger basis set (6-31+G* instead of 6-31G*) show no significative changes in the solvent-induced frequency shifts, although absolute values can change up to 40 cm^{-1} (for the bands at highest frequencies).

Similarly to M1, in the quantitative comparison between calculated and experimental IR absorption coefficients we shall possibly call "bands" also ensembles of overlapping peaks. The integration ranges and the label of each band are reported in Table 5.

The correlation between calculated and experimental vibrational coefficients is illustrated by Figure 6. As can be seen, the agreement is not very good. In particular, as already noted for M1, absolute infrared intensities are overestimated and

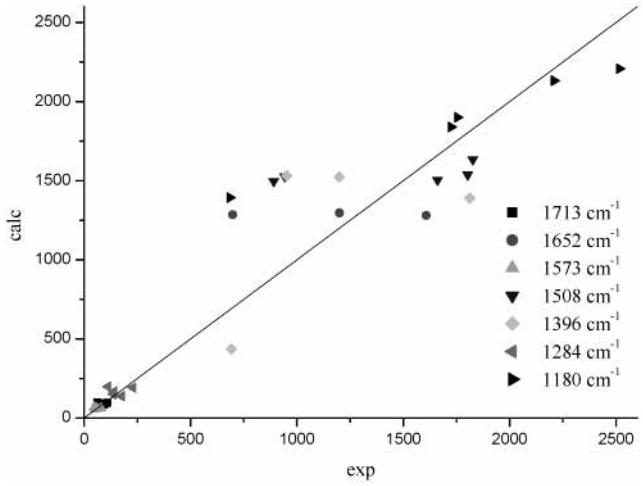

Figure 7. Comparison between calculated (calc) and experimental (exp) IR absorption intensities for different bands of M2 in different solvents. Calculated results are scaled as explained in the text. Values are in km mol^{-1}.

solvent effects are underestimated. The same procedure used above for M1 to decouple the quality of the results from the level of calculation gives the findings depicted in Figure 7. The scattering of the values is reduced, but the agreement between calculated and experimental solvent effects on A^{sol} is still unsatisfactory. Various reasons can be responsible for this behavior:

1. Due to the relatively high concentrations used in the experiments (10^{-5} mol cm^{-3}), we cannot rule out some form of aggregation between solute molecules in the solution. If this is the case, one of the main assumptions of our model (infinitely diluted solutions) breaks down. This aggregation, if present, would surely be strongly solvent dependent, and thus, its effects on infrared absorption would probably hide electrostatic effects taken into account by our theory.

2. The procedure that should decouple the level of accuracy of the QM calculation and the solvation model effect is only approximated, and thus, it is possible that the discrepancies arise from the inability of DFT to treat this particular system. Although our methodology for taking into account solvation effects on IR intensities can be, in principle, extended to other levels of calculation (such as, for example, Möller−Plesset (MP) perturbation theory, multiconfigurational self-consistent field, or configuration interaction), the actual implementation is limited to HF and DFT. Thus, we could not check the effect of other levels of calculation on our results. In addition, due to the high computational cost required by this system, an extensive investigation of other functionals besides B3LYP and other basis sets was not possible. We have performed some tests with the larger 6-31+G* basis set, but calculated results do not significatively improve.

3. Our model accounts only for electrostatic interactions between solute and solvent. Dispersion and repulsion are not considered, as well as other kinds of specific interactions.

4. All the calculations are based on the double (mechanical and electrical) harmonic approximation. Although this assumption can have consequences, for example, by mixing normal modes (mechanical anharmonicity) with similar frequencies and redistributing their intensity, it is unlikely that a behavior common to almost all bands (underestimation of solvent effects) depends on anharmonicity only, which would instead act differently on different bands.

4.2. Raman Scattering Activity. *4.2.1. M1.* As said above in the Computational Details section, we have focused the

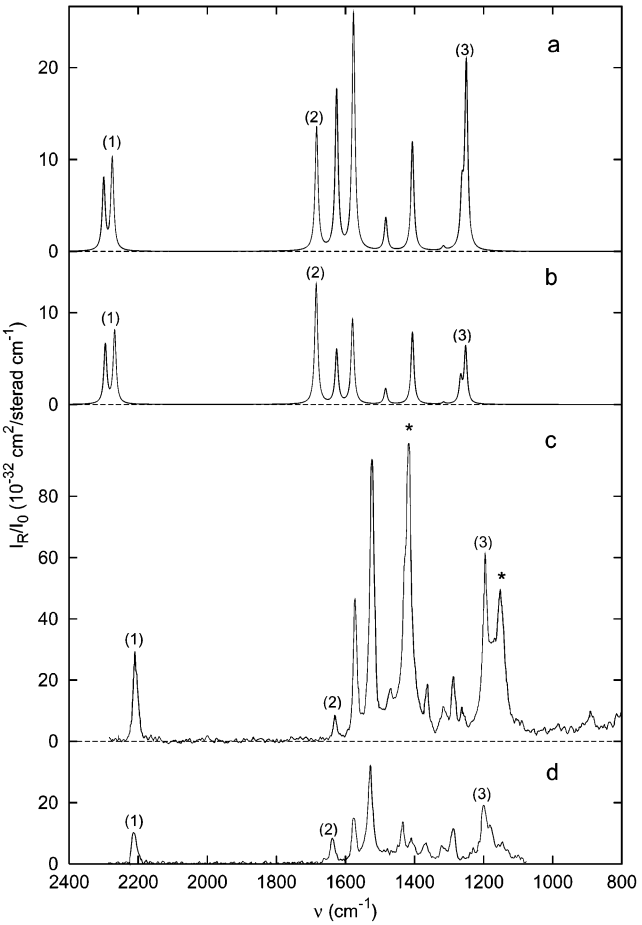

Figure 8. Calculated and experimental Raman spectra of M1 in dichloromethane (a, c) and methanol (b, d). All the calculated spectra are obtained by considering Lorentzian-shaped bands with a bandwidth of 10 cm^{-1}.

analysis only on some selected bands of the Raman spectrum. From a computational point of view, this means that we have performed numerical derivatives of $\bar{\alpha}^*$ only for the normal coordinates assigned to the bands experimentally investigated (the assignment has been based on the IR spectrum). Obviously, such a choice, which is computationally very convenient, makes the comparison between experimental and calculated spectra incomplete. However, for the sake of completeness, we report in Figure 8 simulated (10 normal modes) and experimental Raman spectra of M1 in dichloromethane and in methanol. Such solvents were chosen, as they have different polarity and their Raman spectra overlap only slightly with that of M1. The band shapes of the calculated spectrum have been assumed Lorentzian with a bandwidth of 10 cm^{-1}. First, we note that the calculated spectra are less intense than the experimental ones. We shall come back to this point in the next paragraph, where we shall quantitatively compare calculated and experimental scattering activities. As for the IR spectrum, we obtain in the calculation a splitting of the nitrile stretching peak (1) which is not present in the experimental spectrum. In the simulated spectrum in CH_2Cl_2, the relative intensity of peak (2) is strongly overestimated, whereas the experimental region between 1400 and 1600 cm^{-1} is well described by the calculation. The relative intensity of peak (3) is also well reproduced. Moving from dicholoromethane to methanol, the most evident change in the experimental spectrum is the increase in the relative intensity of peak (2), which is correctly reproduced by the calculation. However, as the relative intensity of peak (2) was already overestimated in the simulated spectrum in CH_2Cl_2, we predict again a too large relative intensity for peak (2).

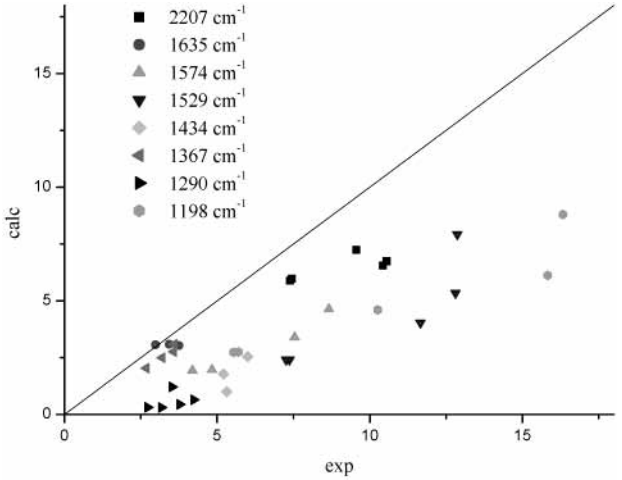

Figure 9. Comparison between calculated (calc) and experimental (exp) Raman scattering activities $|R|$ for different bands of M1 in different solvents. Values are in 10^{-4} cm^2 g$^{-1/2}$.

TABLE 6: Integration Ranges for the Raman Scattering Activities of the Various Bands of M1[a]

band (cm^{-1})	range (cm^{-1})	band (cm^{-1})	range (cm^{-1})
2207	2223-2192	1434	1480−1424
1635	1653−1626	1367[b]	1389−1357[b]
1574	1598−1562	1290	1304−1280
1529	1561−1515	1198	1231−1170

[a] The values refer to the Raman spectrum in acetonitrile. [b] Values for methanol.

Absolute Raman intensities are usually affected by a larger experimental error than that for vibrational absorption coefficients. However, such errors (10−20% in the present case) are smaller than solvent induced effects and thus the comparison between experiments and calculations can be meaningful.

Raman scattering activities will be expressed through $|R|$ defined in eq 6. Each experimental value groups together contributions of different vibrational modes, as for IR. In particular, we have taken care of showing calculated results which group together the same modes as experimental values; only in this way, in fact, are experimental and calculated data comparable. In Table 6 we report the integration ranges for each band, labeled as for IR.

The correlation between calculated and experimentally determined $|R|$ values is shown in Figure 9. First, we note that calculated results underestimate the values of $|R|$ by approximately 50%. In addition, the scattering of data is higher in this case than that for vibrational absorption coefficients. Noticeably, one of the bands with the smallest calculation−experiment discrepancy is the CN stretching, which, as discussed above, should be free of complications such as intensity redistribution between adjacent bands; thus, its computational prediction should be easier.

A possible reason for the underestimation is the relatively small basis set. We (and others)[6,19,29] have verified that, in the case of small molecules, larger basis sets (for example, the one by Sadlej,[30] which should be particularly suitable for Raman intensities because it is tailored for the molecular polarizability) give greater absolute values of the Raman scattering intensity. We have tried to perform calculations by using the Sadlej basis, but we experienced problems in SCF convergence, probably related to basis set overcompleteness.

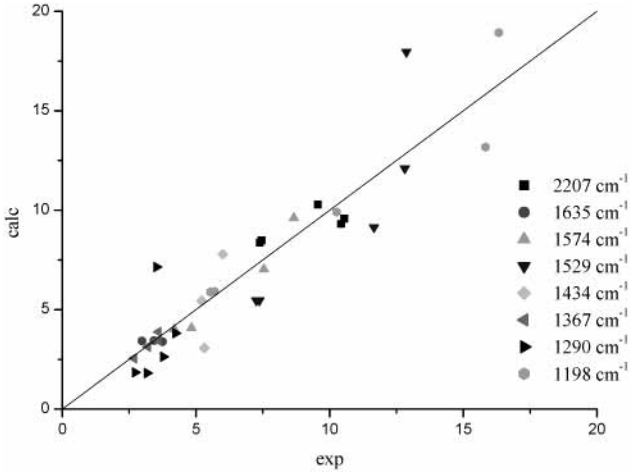

Figure 10. Comparison between calculated (calc) and experimental (exp) Raman scattering activities $|R|$ for different bands of M1 in different solvents. Calculated results are scaled as explained in the text. Values are in 10^{-4} cm^2 g$^{-1/2}$.

TABLE 7: Integration Ranges for the Raman Scattering Activities of the Various Investigated Bands of M2[a]

band (cm^{-1})	range (cm^{-1})	band (cm^{-1})	range (cm^{-1})
1713	1727−1702	1284	1314−1271
1573	1595−1564	1186	1231−1135
1508	1547−1486		

[a] The values refer to the Raman spectrum in chloromethane

To approximately decouple the calculation level from the solvent model, we have applied to $|R|$ the same scaling procedure presented above for the vibrational absorption coefficient. Again, the use of such a procedure is based on the consideration that simplest solvation theories[31] use multiplicative factors to introduce solvent effects starting from in-vacuo Raman activities. Figure 10 presents the experiment−calculation correlation graph after the scaling. This figure shows that the main reason for the large scattering of Figure 9 was not due to lack of linearity among data belonging to the same band but to different linear coefficients for each band. After scaling, a fairly good correlation between calculations and experiments is observed, apart from some points referring to the band at 1529 cm^{-1}. The band spanning the largest range of $|R|$ (1198 cm^{-1}) shows a quite good experiment−theory correlation.

4.2.2. M2. In the case of M2, we will not perform any comparison between simulated and experimental spectra. In fact, since we are using a model molecule bearing methyl groups instead of ethyl groups, we know from the very beginning that some bands, which are important to reproduce the qualitative appearance of the experimental spectrum, cannot be correctly predicted. In addition, the appearance of the experimental spectrum of M2 in polar solvents (acetonitrile and nitromethane) is dominated by the solvent bands, not allowing for an easy comparison with the calculation (we recall that in Raman spectroscopy it is not straightforward to subtract the pure-solvent spectrum directly from the solution one, as can be done for IR).

As before, we will compare the Raman scattering activities (expressed as $|R|$) obtained from calculations and from experiments. Table 7 collects the integration ranges (in chloromethane) for the considered bands.

The correlation between calculated and experimental results for $|R|$ is shown in Figure 11. The scattering of the data is quite large and not too different from what is observed for M1. Again, calculations underestimate experiments, but for at least two bands (1713 and 1573 cm^{-1}), the agreement is pretty good. By

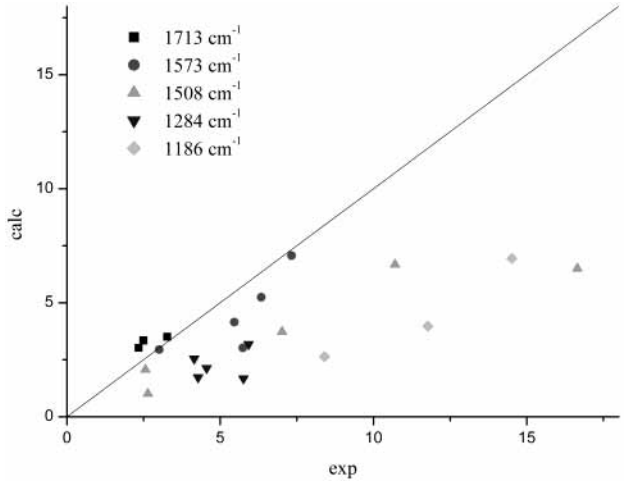

Figure 11. Comparison between calculated (calc) and experimental (exp) Raman scattering activities $|R|$ for different bands of M2 in different solvents. Values are in 10^{-4} cm^2 g$^{-1/2}$.

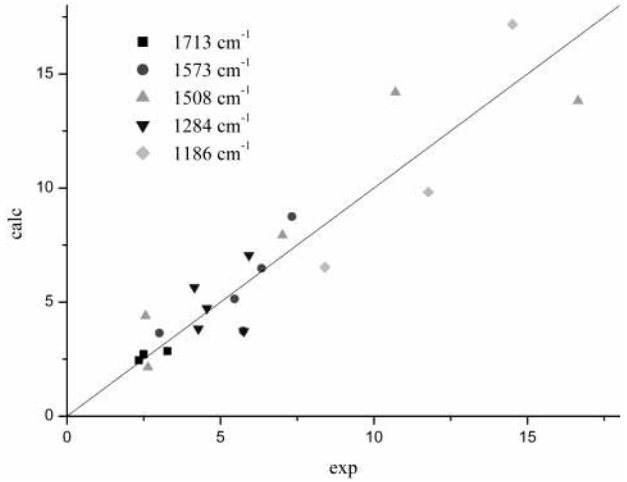

Figure 12. Comparison between calculated (calc) and experimental (exp) Raman scattering activities $|R|$ for different bands of M2 in different solvents. Calculated results are scaled as explained in the text. Values are in 10^{-4} cm^2 g$^{-1/2}$.

applying the scaling procedure (see above), we obtain the plot reported in Figure 12, where the scattering of the data is noticeably reduced. The agreement between calculations and experiments is fairly good, at least of the same quality as that for M1 (see Figure 10).

In light of the results obtained for IR (see section 4.1.2), this relatively good agreement is quite surprising. However, we remark that, among the bands considered in Figure 12, the ones at 1713, 1573, and 1284 cm^{-1} have small IR absorption coefficients, only slightly solvent-sensitive. Thus, since the comparisons for IR and Raman mainly refer to different bands, it is possible that the quality of the description is different in the two cases. In particular, looking at normal modes associated with these bands, it is found only negligible components due to motions of the fictitious methyl groups (which, we recall, in our model molecule replace the ethyl groups of the actual molecule) are involved. In contrast, the other bands contain small but not negligible components of methyl motions. Besides this observation regarding the methyl groups, we were not able to find other simple correlations between the nature of the normal modes and the quality of the agreement between theory and experiment for a given band (the graphical representation of the normal modes is available as Supporting Information). However, as a general remark, it is reasonable that the scaling

TABLE 8: Calculated Values of the Bond Length Alternation Parameter (BLA) for M1 in Vacuo and in Different Solvents

medium	vac	C_6H_6	$CHCl_3$	CH_2Cl_2	CH_3CN	CH_3OH
BLA (Å)	0.0428	0.0275	0.0161	0.0108	0.0042	0.0045

TABLE 9: Calculated Values of the Bond Length Alternation Parameter (BLA) for M2 in Vacuo and in Different Solvents

medium	vac	CCl_4	$CHCl_3$	CH_2Cl_2	CH_3CN	CH_3NO_2
BLA (Å)	0.0454	0.0309	0.0215	0.0155	0.0101	0.0101

procedure discussed above works better for bands involving only one kind of vibrational coordinate (such as the bands at 1713, 1573, and 1284 cm^{-1}). In fact, when different vibrational coordinates (e.g. skeletal and carbonyl stretching in the case of the band at 1652 cm^{-1}) contribute to the same band, each coordinate should have its own scaling factor, while we can only determine an "averaged" factor.

5. Bond Length Alternation and Calculated Vibrational Intensities

The bond length alternation (BLA) can be defined as the average of the difference in the length between adjacent carbon−carbon bonds in the polymethyne [$(CH)_n$] bridge between the push and the pull groups. Such a quantity has been widely used to rationalize the trends of linear and nonlinear optical properties of push−pull molecules, since it is a measure of the conjugation along the π-bond chain.[2] In Tables 8 and 9 we report the calculated values for M1 and M2 in the gas phase and in the various solutions here considered.

We note that our model predicts a decrease of the BLA (i.e., an increase in the conjugation of the chain) in passing from in vacuo to solution and then from nonpolar to polar solvents. This is the expected trend, since solvent effects (in particular, for polar solvents) increase the relative stability of the zwitterionic resonance structure in comparison with the neutral one.

From what we have discussed in the previous sections, it comes out that our calculations overestimate IR intensities and in parallel underestimate Raman activities. In particular, large errors are associated with vibrational modes involving the vibration of the carbon−carbon chain. IR intensities and Raman activities are obtained respectively as derivatives of the dipole moment and of the polarizability with respect to normal coordinates. For vibrations of the C−C chain, such normal coordinates imply variations of the BLA. Thus, IR intensities and scattering activities of these vibrations are related to the derivatives of the dipole moment and of the polarizability with respect to the BLA. The behavior of the dipole moment and molecular polarizability (and their vibrational contributions, strictly connected to IR and Raman intensities) as a function of the degree of conjugation of the π-bond chain has been investigated by different authors (see, for example, ref 32 and references therein).

Focusing on M1, the bands having the largest components due to motions of the chain (those at 1530 and 1576 cm^{-1}) show an increase in the IR intensity and conversely a decrease in the Raman activity (independently of local field effects) in passing from nonpolar to polar solvents. In other words, we found for M1 that a decrease in BLA corresponds to an increase in IR intensities and to a decrease in Raman activities. Given such a behavior, we tentatively propose the following as one of the reasons for the discrepancy between calculations and experiments: the level of calculation that we have used (DFT with the hybrid B3LYP functional) underestimates the BLA (i.e., it overestimates the conjugation); due to this underestimation, we obtain, in light of the trends noted above, an overestimation of the calculated IR intensities and an underestimation of the Raman activities.

TABLE 10: Calculated Values of the Bond Length Alternation Parameter (BLA) for M1 in Vacuo at Different QM Levels[a]

level	HF	MP2	B3LYP	BLYP
BLA (Å)	0.0803	0.0499	0.0428	0.0353

[a] The same basis set (6-31+G*) has been used for all the calculations.

To further check this issue, still keeping the 6-31+G* basis set, we have repeated geometry optimizations for M1 in the gas phase at the HF and MP2 levels, as well as at the DFT level with the BLYP functional (see Table 10). As can be seen, DFT gives lower values for the BLA in comparison with both HF and MP2. Notice, in addition, that the BLYP (that contains no Hartree−Fock exchange) value is even lower than the B3LYP one. These findings agree with similar observations previously reported in the literature (see, for example, refs 33−37) with regard to various alternating single−double bond systems (but in the case of nonsubstituted polyenes, comparable results for B3LYP and MP2 have been obtained).[38] Thus, possible disagreements between calculated and experimental values may be due to the limited capability of DFT to accurately describe some aspects of the structure of the molecule. In addition, the use of DFT for the calculation of electric properties such as dipole moments and static polarizabilities, related to IR and Raman intensities, has been questioned for large push−pull systems.[39] However, for molecules of the size of M1 and M2, DFT still represents the best compromise between accuracy and feasibility.

6. Conclusions

In this article, we have presented a comparison between experimental and calculated results for vibrational properties (frequencies, IR absorption intensities, and Raman scattering activities) of two push−pull molecules in several solvents. The computational methodology used is based on the PCM description of the solution, with the solute treated quantum-mechanically at the DFT level. The harmonic approximation has been exploited in all the calculations. As a general note, our calculated results seem to overestimate infrared absorption coefficients and to underestimate Raman scattering activities in comparison with experiments. However, by using an approximate procedure for decoupling the QM level of calculation from the results of the solvation model, we found that solvent effects on absorption and scattering intensities are predicted quite well, with the possible exception of IR intensities for M2. A number of reasons for discrepancies between calculated and experimental results have been discussed. Finally, we have investigated the variation of an important structural parameter of push−pull molecules (the BLA) as a function of the solvent, and on the basis of this parameter, we have suggested one of the possible reasons for the observed overestimation of IR intensity and underestimation of Raman activity.

Acknowledgment. S.C., C.C., and J.T. thank MIUR (Ministero dell'Istruzione, Università e Ricerca) and Gaussian, Inc. for financial support.

Supporting Information Available: Pictures of the normal modes of M1 and M2 of interest in this study. This material is available free of charge via the Internet at http://pubs.acs.org.

References and Notes

(1) Meyers, F.; Marder, S. R.; Perry, J. W. In *Chemistry of Advanced Materials—An Overview*; Interrante, L. V., Hampden-Smith, M. J., Eds.; Wiley-VCH: New York, 1998.

(2) (a) Marder, S. R.; Perry, J. W.; Tiemann, B. G.; Gorman, C. B.; Gilmour, S.; Biddle, S. L.; Bourhill, G. *J. Am. Chem. Soc.* **1993**, *115*, 2524. (b) Bourhill, G.; Bredas, J.-L.; Cheng, L.-T.; Marder, S. R.; Meyers, F.; Perry, J. W.; Tiemann, B. G. *J. Am. Chem. Soc.* **1994**, *116*, 2619.

(3) (a) Zuliani, P.; Del Zoppo, M.; Castiglioni, C.; Zerbi, G.; Marder, S. R.; Perry, J. W. *J. Chem. Phys.* **1995**, *103*, 9935. (b) Del Zoppo, M.; Castiglioni, C.; Zuliani, P.; Razelli, A.; Tommasini, M.; Zerbi, G.; Blanchard-Desce, M. *J. Appl. Polym. Sci.* **1998**, *70*, 1311. (c) Del Zoppo, M.; Castiglioni, C.; Zuliani, P.; Zerbi, G. In *Handbook of Conducting Polymers*; Skotheim, T. A., Elsenbaumer, R. L., Reynolds, J. R., Eds.; Dekker: New York, 1998; Chapter 28.

(4) Cammi, R.; Cappelli, C.; Corni, S.; Tomasi, J. *J. Phys. Chem. A* **2000**, *104*, 9874; *E* **2002**, *106*, 6426.

(5) Cappelli, C.; Corni, S.; Cammi, R.; Mennucci, B.; Tomasi, J. *J. Chem. Phys.* **2000**, *113*, 11270.

(6) Corni, S.; Cappelli, C.; Cammi, R.; Tomasi, J. *J. Phys. Chem.* **2001**, *105*, 8310.

(7) Cappelli, C.; Corni, S.; Tomasi, J. *J. Chem. Phys.* **2001**, *115*, 5531.

(8) Cappelli, C.; Corni, S.; Tomasi, J. *J. Phys. Chem.* **2001**, *105*, 10807.

(9) (a) Miertuš, S.; Scrocco, E.; Tomasi, J. *Chem. Phys.* **1981**, *55*, 117. (b) Cammi, R.; Tomasi, J. *J. Comput. Chem.* **1995**, *16*, 1449.

(10) Tomasi, J.; Persico, M. *Chem. Rev.* **1994**, *94*, 2027.

(11) Craig, D. P.; Thirunamachandran, T. *Molecular Quantum Electrodynamics*; Academic Press: London, 1984.

(12) (a) Böttcher, C. J. F. *Theory of Electric Polarization*; Elsevier: Amsterdam, 1973; Vol. I. (b) Böttcher, C. J. F.; Bordewijk, P. *Theory of Electric Polarization*; Elsevier: Amsterdam, 1978; Vol. II.

(13) Tang, J.; Albrecht, A. In *Raman Spectroscopy*; Szymanski, H., Ed.; Plenum Press: New York, 1970; Vol. 2.

(14) Long, D. A. *The Raman effect*; Wiley: New York, 2002.

(15) Quinet, O.; Champagne, B. *J. Chem. Phys.* **2001**, *115*, 6293.

(16) Castiglioni, C.; Tommasini, M.; Del Zoppo, M. *J. Mol. Struct.* **2000**, *521*, 137.

(17) Frisch, M. J.; Trucks, G. W.; Schlegel, H. B.; Scuseria, G. E.; Robb, M. A.; Cheeseman, J. R.; Zakrzewski, V. G.; Montgomery, J. A.; Stratmann, R. E.; Burant, J. C.; Dapprich, S.; Millam, J. M.; Daniels, A. D.; Kudin, K. N.; Strain, M. C.; Farkas, O.; Tomasi, J.; Barone, V.; Mennucci, B.; Cossi, M.; Adamo, C.; Jaramillo, J.; Cammi, R.; Pomelli, C.; Ochterski, J.; Petersson, G. A.; Ayala, P. Y.; Morokuma, K.; Malick, D. K.; Rabuck, A. D.; Raghavachari, K.; Foresman, J. B.; Ortiz, J. V.; Cui, Q.; Baboul, A. G.; Clifford, S.; Cioslowski, J.; Stefanov, B. B.; Liu, G.; Liashenko, C. A.; Piskorz, P.; Komaromi, I.; Gomperts, R.; Martin, R. L.; Fox, D. J.; Keith, T.; Al-Laham, M. A.; Peng, C. Y.; Nanayakkara, A.; Challacombe, M.; Gill, P. M. W.; Johnson, B.; Chen, W.; Wong, C. M. W.; Andres, J. L.; Gonzalez, C.; Head-Gordon, M.; Replogle, E. S.; Pople, J. A. *Gaussian 99, Development Version*, Revision B09+; Gaussian Inc.: Pittsburgh, PA, 2000.

(18) Halls, M. D.; Schlegel, H. B. *J. Chem. Phys.* **1998**, *109*, 10587.

(19) Halls, M. D.; Schlegel, H. B. *J. Chem. Phys.* **1999**, *111*, 8819.

(20) (a) Cancès, E.; Mennucci, B. *J. Math. Chem.* **1998**, *23*, 309. (b) Cancès, E.; Mennucci, B.; Tomasi, J. *J. Chem. Phys.* **1997**, *107*, 3031. (c) Mennucci, B.; Cancès, E.; Tomasi, J. *J. Phys. Chem. B* **1997**, *101*, 10506. (d) Mennucci, B.; Cammi, R.; Tomasi, J. *J. Chem. Phys.* **1998**, *109*, 2798.

(21) Tomasi, J.; Cammi, R.; Mennucci, B.; Cappelli, C.; Corni, S. *Phys. Chem. Chem. Phys.* **2002**, *4*, 5697.

(22) (a) Cancès, E.; Mennucci, B. *J. Chem. Phys.* **1998**, *109*, 249. (b) Cancès, E.; Mennucci, B.; Tomasi, J. *J. Chem. Phys.* **1998**, *109*, 260.

(23) Mennucci, B.; Cammi, R.; Tomasi, J. *J. Chem. Phys.* **1999**, *110*, 6858.

(24) Kato, Y.; Takuma, H. *J. Chem. Phys.* **1971**, *54*, 5398.

(25) Scott, A. P.; Radom, L. *J. Phys. Chem.* **1996**, *100*, 16502.

(26) Onsager, L. *J. Am. Chem. Soc.* **1936**, *58*, 1486.

(27) (a) Chako, N. Q. *J. Chem. Phys.* **1934**, *2*, 644. (b) Polo, S. R.; Wilson, M. K. *J. Chem. Phys.* **1955**, *23*, 2376. (c) Clifford, A. A.; Crawford, B. *J. Phys. Chem.* **1966**, *70*, 1536. (d) Hirota, E. *Bull. Chem. Soc. Jpn.* **1954**, *27*, 295. (e) Mallard, W. C.; Straley, J. W. *J. Chem. Phys.* **1957**, *27*, 877. (f) Person, W. B. *J. Chem. Phys.* **1958**, *28*, 319. (g) Buckingham, A. D. *Proc. R. Soc. (London)* **1958**, *A248*, 169; **1960**, *A255*, 32. (h) Mirone, P. *Spectrochim. Acta* **1966**, *22*, 1897.

(28) Cappelli, C.; Silva, C. O.; Tomasi, J. *THEOCHEM* **2001**, *544*, 191.

(29) Van Caillie, C.; Amos, R. D. *Phys. Chem. Chem. Phys.* **2000**, *2*, 2123.

(30) (a) Sadlej, A. J. *Collect. Czech. Chem. Commun.* **1988**, *53*, 1995. (b) Sadlej, A. J. *Theor. Chim. Acta* **1991**, *79*, 123.

(31) (a) Nestor, J. R.; Lippincott, E. R. *J. Raman Spectrosc.* **1973**, *1*, 305. (b) Fini, G.; Mirone, P.; Patella, P. *J. Mol. Spectrosc.* **1968**, *28*, 144.

(32) Kirtman, B.; Champagne, B.; Bishop, D. M. *J. Am. Chem. Soc.* **2000**, *122*, 8007.

(33) Bifone, A.; de Groot, H. J. M.; Buda, F. *Chem. Phys. Lett.* **1996**, *248*, 165.

(34) Choi, C. H.; Kertesz, M.; Karpfen, A. *J. Chem. Phys.* **1997**, *107*, 6712.

(35) Paizs, B.; Tajkhorshid, E.; Suhai, S. *J. Phys. Chem. B* **1999**, *103*, 5388.

(36) Buda, F.; Giannozzi, P.; Mauri, F. *J. Phys. Chem. B* **2000**, *104*, 9048.

(37) Geskin, V. M.; Bredas, J. L. *Int. J. Quantum Chem.* **2003**, *91*, 303.

(38) Schettino, V.; Gervasio, F. L.; Cardini, G.; Salvi, P. R. *J. Chem. Phys.* **1999**, *110*, 3241.

(39) Champagne, B.; Perpète, E. A.; Jacquemin, D.; van Gisbergen, S. J. A.; Baerends, E.-J.; Soubra-Ghaoui, C.; Robins, K. A.; Kirtman, B. *J. Phys. Chem. A* **2000**, *104*, 4755.